

# Distribution Grid Monitoring: challenges and related complexity

**Abstract.** Monitoring of distribution grids is an increasingly relevant topic in the smart grid framework. The straightforward migration of transmission system technologies in this application area is practically often unfeasible. Functional specifications that the monitoring in distribution network should provide are deduced here from the features of the new distribution systems. In light of this, possible techniques for dynamic phasor measurements and state estimation for distribution networks are critically presented.

**Streszczenie.** W koncepcji sieci inteligentnych nadzór sieci staje się zagadnieniem o rosnącym znaczeniu. Bezpośrednie przeniesienie technologii systemów transmisyjnych do inteligentnych systemów rozdzielczych jest jednak często praktycznie niewykonalne. Operacyjne właściwości, które takie systemy powinny zapewniać wyprowadzone są w tym artykule z właściwości nowych systemów rozdzielczych. Zgodnie z takim punktem widzenia, w artykule analizuje się możliwe technologie pomiarów fazowych oraz metody przewidywania stanu systemów rozdzielczych. (**Nadzór w systemach rozdzielczych: wyzwania i złożoność**)

**Keywords:** power distribution, measurement uncertainty, power system measurement

**Słowa kluczowe:** Rozdział mocy, niepewność pomiarowa, pomiary energetyczne.

## Introduction

This paper presents a review of the challenges related to distribution grid monitoring. Starting from an overview of the reasons why Distribution Grid Monitoring is becoming a new important area of application, the analysis focuses on identifying the fundamental changes with respect to the traditional application in Transmission systems. Starting from these differences and from the corresponding challenges, an analysis of possible new approaches is proposed. Theoretical proposal are analysed also in the context network simulation examples.

## Features of distribution grid monitoring

Grid Monitoring is typically performed for transmission system operation. A fundamental element of the grid monitoring is the State Estimation process. State Estimation aims at calculating the voltage profile, in terms of magnitude and phase, for every node of the network.

Typical input of the State Estimator is a set of measurements, of different nature, such as active power flows and injections, reactive power, RMS values. Typical output is the voltage profile in terms of RMS and phase, where the phase is referred to one specific reference bus.

The state estimation process, whose typical structure is laid out in Figure 1, comprises setting up the problem, to be solved numerically, in terms of topology of the grid, parameters of the model of the individual components, accuracy of the measurements, and organizing the input data, usually collected through a SCADA system. The state estimation process, then, comprises post-processing steps for bad data detection, validation of topology and parameters.

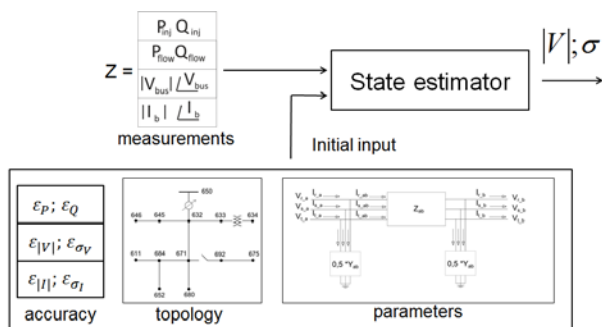


Fig.1. Typical structure of the state estimator

A commonly adopted method for state estimation is the Weighted Least Square algorithm (WLS), which consists in the minimization of the residuals, weighted on factors that usually express the goodness of the measurement in terms of measurement uncertainty. A summary scheme of the WLS is shown in Figure 2.

In this process, state  $x$  is iteratively updated to minimize  $J$ , usually starting from the initial values of  $x=1pu;0^\circ$  :

$$J = \sum_{i=1}^N W_i \cdot res_i^2$$

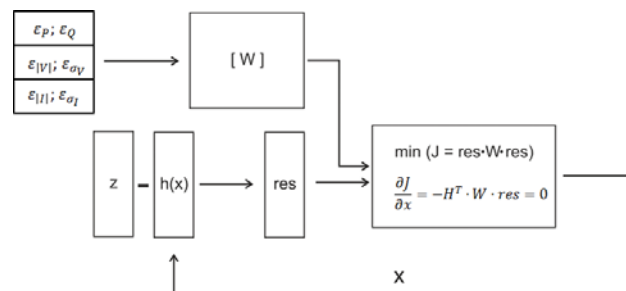


Fig.2. Scheme of the weighted least square algorithm

Monitoring that relies on redundant measurements and state estimation is not normally adopted for distribution grids and not even considered feasible. Actually, until recent times it was not even really needed: in fact the distribution system has been passive and not automated and monitoring would have yielded minimal benefit, particularly to the Distribution System Operators.

The growing presence of distributed energy resources though turning the distribution system to an active grid, calls for Monitoring also for the Distribution System. The reasons are various.

Consider voltage profile to estimate operating range of equipment. This is particularly interesting to assure proper aging of the components in the field but also to assure that the voltage is in every node compliant with the operating standard. This second element connects directly to the more general issue of detection and identification of power quality issue, and particularly in view of actively addressing them. Fault detection, identification, location and system restoration.

And looking into applications further away in the future, monitoring is necessary for the coordination of resources, in form of Virtual Power Plant, in terms of Energy Networks interaction for exploiting multi-physics energy storage

capacities, and finally for supporting transmission system operation.

In the majority of cases the availability of measurement sources in distribution grids is at the moment quite limited, and it is not reasonable to assume that the situation will change dramatically in the short term.

Some feature change common to all power grids are summarized in Figure 3 and 4, with emphasis on dynamic behaviour. In particular, the presence of a large number of generators with small and negligible inertia (such as power electronic interfaced generators with no rotating mass) results in fast dynamics affecting also stability and setting the requirement for much faster and tighter control and monitoring schemes.

The steady-state or quasi steady-state assumption cannot be considered to hold in a scenario, where the resources are either, subject to natural variability (like renewable sources) or arbitrary behaviours (like decisions of the owner of the resources). A more appropriate system representation and definition of system states are needed.

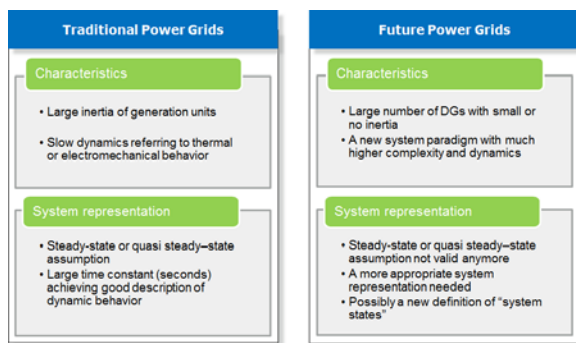


Fig.3. Summary of grid features changes affecting monitoring needs and requirements

Some developments in this direction are already on the way, at least to determine the challenges specific to distribution networks.

In first place, the model definition requires the determination of the actual Dynamic Range that is practically reasonable to assume in distribution networks. Furthermore, models refer to system variables besides components, and performance characterization.

In second place, the constellation of measurement devices indispensable for effective monitoring of the distribution grid has to be determined in terms of device type, location, and characteristics. This process must account for exploitation of existing devices and must leverage for what concerns new deployments, on devices that can contribute the most.

Finally, monitoring algorithms specifically designed for distribution systems should be developed. These algorithms may not be simply adopted from transmission system monitoring because of the following particular challenges:

- the size of the problem
- unbalance
- amount and type of available information

With particular reference to phasor (and synchrophasor) measurements, these may fit well the requirements, once a dynamic version is fully defined and metrological requirements consistent with the application are developed.

### Dynamic phasor measurement

To illustrate the challenges of meeting the phasor monitoring requirements in the dynamic environment, the dq0-transformation method, the classical Fourier method and the modified Taylor Fourier approach are compared.

The dq0-transformation can be formulated as:

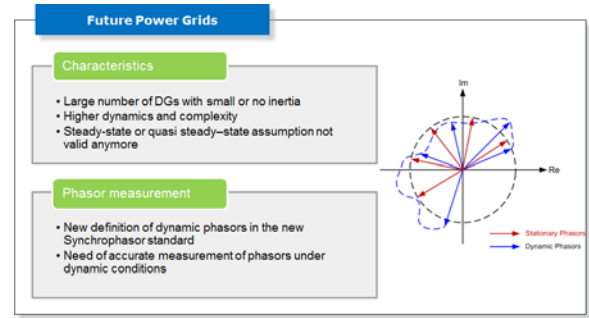


Fig. 1: Future grids and phasor measurement

To illustrate the challenges of meeting the phasor monitoring requirements in the dynamic environment, the dq0-transformation method, the classical Fourier method and the modified Taylor Fourier approach are compared.

The dq0-transformation can be formulated as:

$$(1) \begin{bmatrix} x_d \\ x_q \\ x_0 \end{bmatrix} = \frac{2}{3} \begin{bmatrix} \cos(\theta) & \cos(\theta - \beta \frac{2}{3}\pi) & \cos(\theta + \beta \frac{2}{3}\pi) \\ -\sin(\theta) & -\sin(\theta - \beta \frac{2}{3}\pi) & -\sin(\theta + \beta \frac{2}{3}\pi) \\ \frac{1}{2} & \frac{1}{2} & \frac{1}{2} \end{bmatrix} \begin{bmatrix} x_a \\ x_b \\ x_c \end{bmatrix}$$

with:  $\theta = \omega_0 t$ : the rotating angular speed of the reference frame  $\beta = \pm 1$  denoting the positive or negative sequence.

It follows that the dq-based phasor equivalent to the positive or negative sequence component phasor in stationary balanced sinusoidal conditions, yields:

$$X_{dq0}(t) = x_d(t) + j \cdot x_q(t)$$

According to the classical phasor definition, for a sinusoidal signal with constant amplitude and phase:

$$(2) x(t) = X_m \cos(2\pi f_0 t + \phi)$$

the corresponding phasor representation is:

$$(3) X = \frac{X_m}{\sqrt{2}} e^{j\phi}$$

And it can be computed from the signal samples over the observation window of N samples as:

$$(4) X = \frac{\sqrt{2}}{N} \sum_{n=0}^{N-1} x_n e^{-jn\theta}$$

with  $\Theta = 2\pi/N$ .

Recently, a Taylor-Kalman filter (TFK) approach has been proposed for dynamic phasor estimation in [1] and subsequently modified in [2]. Using the Taylor phasor expansion, a linear dynamic model is formalized to describe the model parameters time-varying behaviour. A Kalman filter is then applied for the estimation. The features of the modified Taylor-Kalman phasor estimator are summarized in Figure 5.

	Short Time Fourier Transform based Approach	Taylor Fourier based Approach
Definition	<ul style="list-style-type: none"> <li>Dynamic phasor = slowly time-varying complex Fourier coefficient assuming rectangular window function</li> </ul> $X_T(t) = \frac{1}{T} \int_{t-T}^t x(\tau) e^{-j\omega_0 \tau} d\tau$	<ul style="list-style-type: none"> <li>Narrow baseband signal presenting power system oscillation</li> </ul> $X(t) = X_m(t) e^{j\omega_0 t}$ <p>approximated by Taylor expansion</p> $X_T(t) = X_1^{(0)} + X_1^{(1)} t + X_1^{(2)} \frac{t^2}{2!} + \dots + X_1^{(k)} \frac{t^k}{k!}$
Features	<ul style="list-style-type: none"> <li>Derivative of dynamic phasor</li> </ul> $\frac{d}{dt} X_T(t) = \left( \frac{d}{dt} x(t) \right) (t) - j\omega_0 X_T(t)$ <ul style="list-style-type: none"> <li>Circuit-based dynamic model</li> </ul>	<ul style="list-style-type: none"> <li>discrete-time state-space model with state transition matrix [xx]</li> </ul> $\begin{bmatrix} X_1^{(0)}(k) \\ X_1^{(1)}(k) \\ \vdots \\ X_1^{(k)}(k) \end{bmatrix} = \begin{bmatrix} 1 & \tau & \dots & \frac{\tau^k}{k!} \\ \vdots & \vdots & \ddots & \vdots \\ 1 & \dots & \frac{\tau^{k-1}}{(k-1)!} & \vdots \\ \vdots & \vdots & \vdots & 1 \\ \vdots & \vdots & \vdots & \vdots \end{bmatrix} \begin{bmatrix} X_1^{(0)}(k-1) \\ X_1^{(1)}(k-1) \\ \vdots \\ X_1^{(k)}(k-1) \end{bmatrix}$ <ul style="list-style-type: none"> <li>Signal-based dynamic model</li> </ul>
Calculation/ Measurement method	<ul style="list-style-type: none"> <li>Sliding window DFT</li> <li>Kalman filter based estimation</li> </ul>	<ul style="list-style-type: none"> <li>Weighted Least Square</li> <li>Kalman filter based estimation</li> </ul>

Fig.5. Summary of comparison of the features of Fourier and Taylor Fourier approaches to phasor estimation

### Case study for comparison

A 3-phase distribution line with 3 different load that connect at different times, shown in Figure 6, is adopted as case study, for the purpose a comparison between the dq0, Fourier and Taylor Fourier approaches.

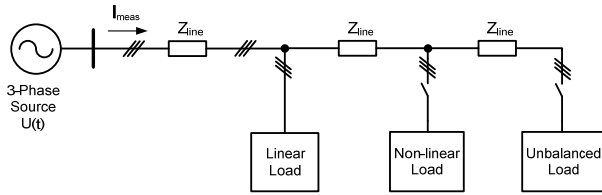


Fig.6. Scheme of case study

The comparison is carried out between current measurements  $I_{meas}$  performed with the different methods. Specific compensations are not applied here as the emphasis is on the direct comparison. The simulation of different scenarios listed below covers the relevant modes of operation:

- Low frequency multi-oscillation
- Load step change
- Unbalance
- Harmonics distortion

Results of the scenarios applied in sequence, as specified in figure, are shown in Figure 7.

The lower plot of Figure 7 shows the amplitude and phase of the current phasors of the direct sequence at the fundamental frequency, calculated with the dq-transformation, the sliding window DFT and the TFT algorithms to the three phase current measurement applied in abc-domain first.

As expected, all methods can estimate fairly well steady state, multi-oscillation and can track the new steady state after load step change condition. Under unbalance and harmonic distortion conditions instead, the dq0-transformation features significant oscillations, which do not appear with the DFT and TFT methods. Thus, the dq0-transformation is not suitable for control purposes such as harmonic compensation and unbalance compensation. Only way to reduce the influence of these negative factors would be to consider not only the first harmonic of such phasor but also further components.

This solution though would increase the complexity of the definition of state for monitoring purpose.

Some specific considerations on each of the scenarios is now presented.

With reference to the low frequency multi-oscillation scenario, Figure 8 shows amplitude and phase of phase a dynamic phasor computed with DFT and TFT methods.

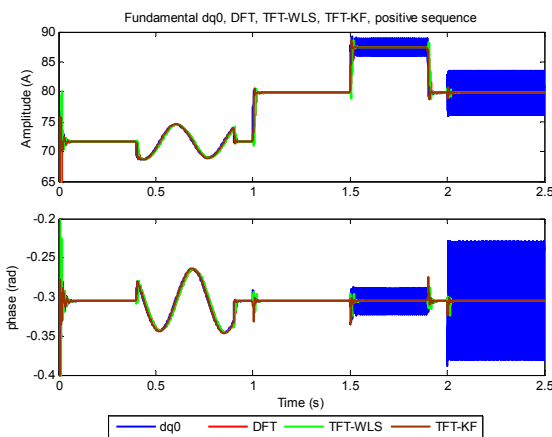


Fig.7. Scheme of case study

It is observed that the phasor calculated by DFT shows an oscillation with the frequency 100Hz at the 2nd-order harmonics due to the off-nominal frequency content under the multi-oscillation conditions.

The TFT based method by approximating the signal with time varying amplitude and phase with higher order Taylor coefficient can suppress the distortion due to off-nominal frequency signal components.

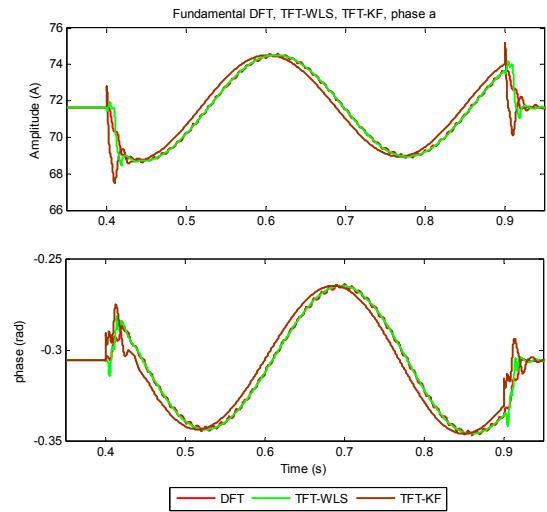


Fig.8. Magnitude and phase of phase a phasor estimated with DFT and TFT algorithms

Notice also the evident delay of the DFT and TFT-WLS due to averaging.

With reference to the load step change scenario, Figure 9 shows a blow up of the positive sequence estimated with the methods under consideration. A step change of +30% of the 3-phase linear load is applied at time 1 s. As expected the dq0 transformation, which can be considered as an instantaneous measurement, shows the fastest tracking performance.

Conversely, the sliding window DFT and TFT-WLS method, due to the averaging calculation, have the slowest tracking showing a lag of one period. With respect to this the Kalman based TFT shows an improved tracking of the magnitude as compared to the TFT-WLS., due to its online adaptive characteristic.

With reference to the unbalance scenario, Figure 10 shows the magnitude and phase of the negative sequence phasor, estimated with the methods under consideration.

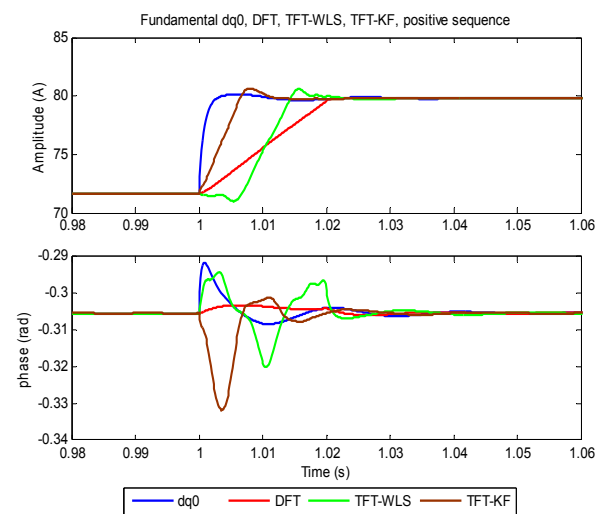


Fig.9. Positive sequence estimate calculated with all methods under consideration during load step change

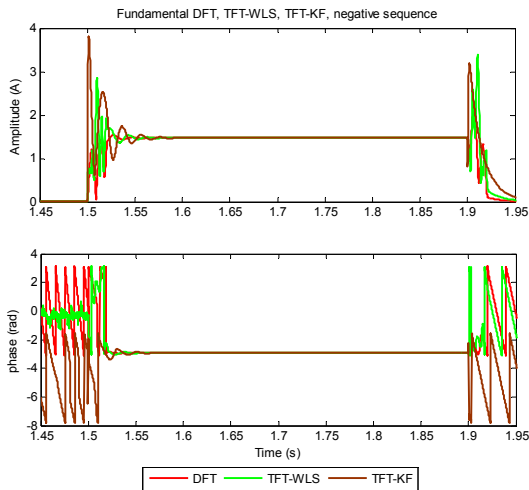


Fig.10. Amplitude and phase of the negative sequence estimate in the unbalance scenario, calculated with DFT and TFL methods

To realize the unbalance, the unbalanced load is set to absorb 50% more current in phase c.

The negative sequence component correctly tracked in steady state by sliding window DFT, TFT-WLS and TFT-KF.

Finally, with reference to the harmonic distortion scenario, Figure 11 shows the amplitude and phase of the estimate of the 5-th harmonic, computed with DFT and TFT methods. The scenario is realized with a nonlinear load that introduces 5th and 7th harmonics in the network. Results show that all three methods can provide good steady state current measurement of the harmonics, with TFT-KF showing the fastest tracking performance.

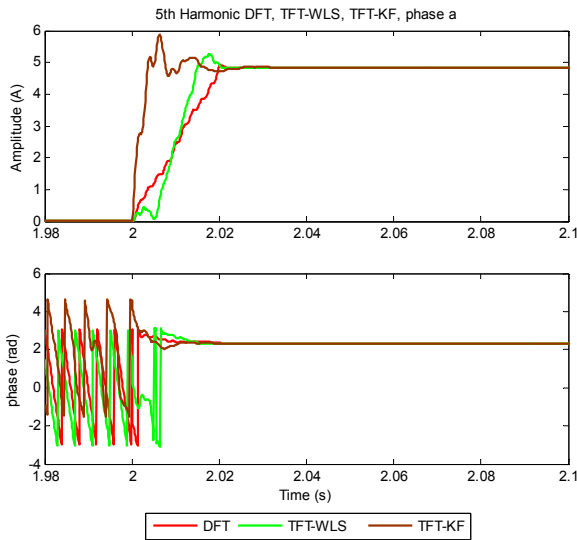


Fig.11. Amplitude and phase of the 5th harmonic phasor, estimated with DFT and TFT methods.

Table 1. functional comparison of the different methods for dynamic phasor estimate

Method	Modeling	Power Electronics Control	Microgrid Control	Power System control
dq0	State space model in dq-domain	Control under sinusoidal condition	Droop control	no
Sliding Window DFT (STFT)	State space modeling phasor domain	Control under non-sinusoidal condition	Power quality control	Power Dispatch
TFT	possible in combination with other method	Control under non-sinusoidal condition	Power quality control	Power Dispatch and Flow Control

Given the performance of the dq0, DFT, and TFT methods, a summary is provided in Table 1 with reference to application areas. The most flexible solution appears to be based on the TFT approaches.

### New approach to dynamic phasors

Different algorithms have been proposed to estimate dynamic phasors, in particular:

- Discrete Fourier Transform (DFT) with error correction of sequential phasors
- Taylor-Fourier Transform
  - Weighted Least Square (WLS) method
  - Kalman Filter based approach with manual adjustment of the Kalman gain, not self-adaptive

Recently a modified Taylor-Kalman Filter was proposed, based on a revised Taylor-Fourier dynamic model for dynamic phasors. This method achieves self-adaptive estimation and it is under investigation for compliance with the dynamic requirements of the newest Synchrophasor standard C37.118.1-2011, C37.118.2-2011.

In Table 2 a summary of signal model, spectrum and phasor model is reported for static and dynamic phasors. Here a dynamic phasor is formalized as baseband representation of the frequency components, with a complex envelope.

Table 2. features of static and dynamic phasor representation

	Stationary	Dynamic
Signal Model	$s(t) = \sum_{m=1}^{N_h} a_m \cos(j\omega_m t + \varphi_m)$ $= \sum_{m=1}^{N_h} \text{Re} \{ p_m e^{j\omega_m t} \}$	$s(t) = \sum_{m=1}^{N_h} a_m(t) \cos(j\omega_m t + \varphi_m(t))$ $= \sum_{m=1}^{N_h} \text{Re} \{ p_m(t) e^{j\omega_m t} \}$
Spectrum representation	<ul style="list-style-type: none"> <li>• Single tone signals at each freq.</li> </ul>	<ul style="list-style-type: none"> <li>• Narrow-band signals around each freq.</li> </ul>
Phasor Definition	<ul style="list-style-type: none"> <li>• Constant amplitude and phase</li> </ul> $p_m = a_m e^{j\varphi_m}$	<ul style="list-style-type: none"> <li>• Time varying amplitude and phase</li> </ul> $p_m(t) = a_m(t) e^{j\varphi_m(t)}$

The principle of the Taylor Fourier Transform consists in approximating the complex envelope function with a truncated Taylor polynomial, hence obtaining a dynamic phasor state vector.

The approximation of the Taylor polynomial representation yields:

$$p(t) = a(t)e^{j\varphi(t)} \Rightarrow \begin{cases} p_K^{(0)}(t) = p_K^{(0)}(t_0) + p_K^{(1)}(t_0)\tau + \dots + p_K^{(K)}(t_0)\frac{\tau^K}{K!} \\ p_K^{(1)}(t) = p_K^{(1)}(t_0) + p_K^{(2)}(t_0)\tau + \dots + p_K^{(K)}(t_0)\frac{\tau^{K-1}}{(K-1)!} \\ \vdots \\ p_K^{(K)}(t) = p_K^{(K)}(t_0). \end{cases}$$

where  $p_K^{(i)}(t)$  represent a component of the dynamic phasor state vector.

The state transition equation in matrix form is:

$$(6) \mathbf{p}_K(t) = \Phi_K(\tau) \mathbf{p}_K(t_0)$$

where:

$$\tau = t - t_0$$

$$\mathbf{p}_K(t) = \begin{bmatrix} p_K^{(0)}(t) & p_K^{(1)}(t) & \dots & p_K^{(K)}(t) \end{bmatrix}^T$$

$$\Phi_K(\tau) = \begin{bmatrix} 1 & \tau & \cdots & \frac{\tau^K}{K!} \\ & 1 & \cdots & \frac{\tau^{K-1}}{(K-1)!} \\ & & \ddots & \vdots \\ & & & 1 \end{bmatrix}$$

Hence, estimating the dynamic phasor state vector means to estimate the Taylor components of the complex envelope.

Considering now the rotating phasor  $r(t)$ :

$$r(t) = p(t)e^{j\omega_1 t}$$

the dynamic model of the truncated rotating phasors and its derivatives yields a more accurate dynamic model describing the complex trajectory of the dynamic phasors:

$$(7) \quad \mathbf{r}_K(t) = \begin{bmatrix} r_K^{(0)}(t) \\ r_K^{(1)}(t) \\ \vdots \\ r_K^{(K)}(t) \end{bmatrix} = e^{j\omega_1 t} \cdot \begin{bmatrix} 1 & 0 & \cdots & 0 \\ j\omega_1 & 1 & \cdots & 0 \\ \vdots & \vdots & \ddots & \vdots \\ (j\omega_1)^K & K(j\omega_1)^{K-1} & \cdots & 1 \end{bmatrix} \cdot \begin{bmatrix} p_K^{(0)}(t) \\ p_K^{(1)}(t) \\ \vdots \\ p_K^{(K)}(t) \end{bmatrix}$$

$$(8) \quad \begin{bmatrix} r_K^{(0)}(t) \\ r_K^{(1)}(t) \\ \vdots \\ r_K^{(K)}(t) \end{bmatrix} = e^{j\omega_1 t} \cdot \begin{bmatrix} p_K^{(0)}(t) \\ p_K^{(1)}(t) \\ \vdots \\ p_K^{(K)}(t) \end{bmatrix}$$

The state transition equation of the truncated rotating phasor vector is:

$$(9) \quad \mathbf{r}_{mK}(t) = e^{j\omega_m \tau} \cdot \mathbf{M}_{mK} \cdot \Phi_K(\tau) \cdot \mathbf{M}_{mK}^{-1} \cdot \mathbf{r}_{mK}(t_0)$$

and finally in discrete form, by considering  $t_0 = (n-1)\tau$  and  $t = n\tau$  with  $\tau =$  sampling time  $T_s$ :

$$(10) \quad \mathbf{r}_{mK}[n] = e^{j\omega_m \tau} \cdot \Psi_{mK}(\tau) \cdot \mathbf{r}_{mK}[n-1]$$

The estimation using the modified Taylor/ Kalman filter is performed through a linear time invariant (LTI) model, represented by the following state equation:

$$(11) \quad \mathbf{x}[n] = \mathbf{A}\mathbf{x}[n-1] + \mathbf{F}\mathbf{v}[n]$$

and measurement equation:

$$(12) \quad \mathbf{x}[n] = \begin{bmatrix} \mathbf{r}_K[n] \\ \hat{\mathbf{r}}_K[n] \end{bmatrix}; \mathbf{A} = \begin{bmatrix} e^{j\omega_1 \tau} \Psi_K(\tau) & 0 \\ 0 & e^{-j\omega_1 \tau} \hat{\Psi}_K(\tau) \end{bmatrix}$$

where:

$$\Theta = [\mathbf{h}^T \mathbf{h}^T], \mathbf{h}^T = [1 \ 0 \ \cdots \ 0]$$

Using standard discrete time Kalman Filter to estimate the rotating phasor vectors based on the LTI model, the calculation of the estimated dynamic phasors and their derivatives yields:

$$(13) \quad \hat{\mathbf{p}}_K[n] = e^{-j\omega_1 n\tau} \cdot \mathbf{M}_K^{-1} \cdot \hat{\mathbf{r}}_K[n]$$

The application of the proposed dynamic phasor estimator is demonstrated in simulation in the following example:

- Modulated test signal
- Amplitude and phase step test
- Frequency ramp test
- Power system test case

The fundamental frequency is  $f_1 = 50\text{Hz}$ , sampling frequency  $f_s = 64 \cdot f_1$ . The Taylor expansion is truncated at order= 2, signal to noise ratio SNR = 60dB.

The test signal can be represented as:

$$s(t) = a(t) \cos(\omega_1 t + \varphi(t))$$

with amplitude and phase modulation:

$$a(t) = a_0 + a_1 \cos(2\pi f_a t)$$

$$\phi(t) = \phi_0 + \phi_1 \cos(2\pi f_\phi t)$$

with parameters:

$$a_0 = 1, \Phi_0 = 1$$

$$a_1 = 0.1, \Phi_1 = 0.1$$

$$f_a = f_\phi = 5 \text{ Hz}$$

The comparison between the „original“ estimation, based on the incorrect model, and the proposed estimation has been presented in literature [3].

Similar effects can be observed in Figure 12, where magnitude, phase, and Total Vector Error (TVE) as defined in the standard on synchrophasor measurement are presented.

The modified TKF achieves better estimation results in steady state despite of a larger transient before the Kalman filter settles. The oscillation behaviour of the "original" TKF in steady state also requires manual adjustment of the filter, as reported in literature.

Results from the dynamic tests of the proposed algorithm are reported in Figure 13 and Figure 14 for the signal  $s(t)$ :

$$(14) \quad s(t) = a \cdot (1 + k_a f_1(t)) \cdot \cos(\omega_0 t + k_\phi f_1(t))$$

with  $k_a=0.1$ ,  $k_\phi = 10 \text{ deg.}$  and  $f_1(t)$  being a step function.

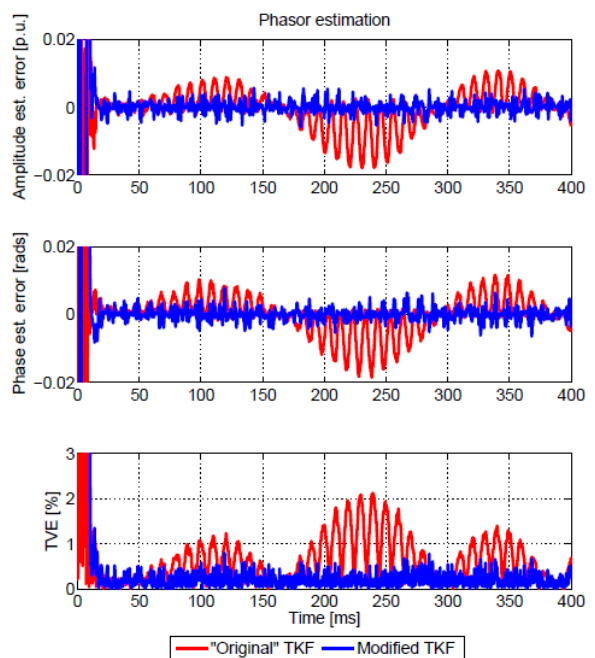


Fig.12. Performance of the modified TKF

Figure 13 shows the response to amplitude step change in terms of amplitude and in terms of TVE, while Figure 14 shows the response to a step change in phase in terms of phase and TVE.

Table 3 reports the performance indices defined in the standard [4], response time, delay time, and overshoot both amplitude and phase step change tests.

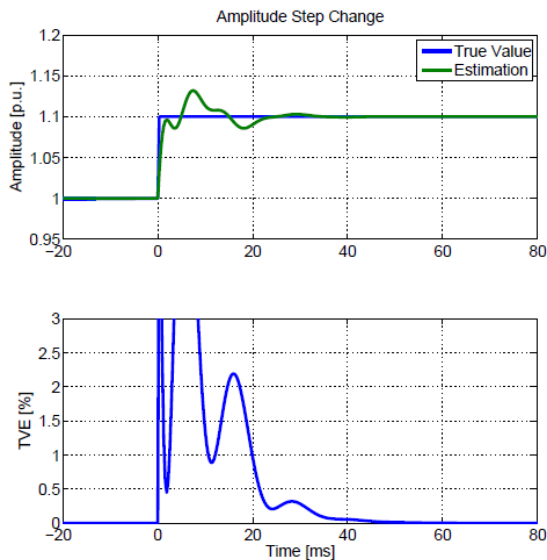


Fig. 13. Response to amplitude step change

While the response time and delay time achieved by the modified TKF fulfil the P-Class requirements of 34ms and 5ms (according to the highest reporting rate of 50fps) in the standard, the overshoot caused by the proposed TKF exceeds the compliance limitation of 5% of the step magnitude. Further investigations are needed to reduce this overshoot.

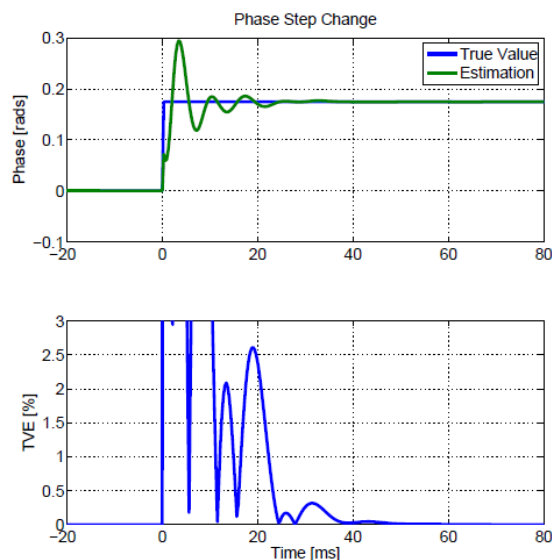


Fig. 14. Response to phase step change

Table 3. performance of the proposed TKF according to the standard definitions

	Response time	Delay time	Overshoot
Amplitude step	19.7 ms	0.6 ms	0.03 [p.u.]
Phase step	22.2 ms	1.6 ms	0.12 [rad]

The next test reported here is the frequency ramp test of test signal  $s(t)$ :

$$(15) \quad s(t) = a \cdot \cos(\omega_0 t + \pi R_f t^2)$$

with

$$a = 1, \omega_0 = 2\pi \cdot 50\text{Hz}, R_f = 1\text{Hz/s},$$

respectively.

A frequency ramp with the range of +2Hz in 2s is applied, as shown in top plot of Figure 15, assuming the

Kalman Filter already settled in steady state. The proposed TKF achieves very small estimation error during the ramping, as shown in the second and third plot of Figure 15. The increasing error is caused by the increasing frequency deviation away from the nominal 50Hz, here not compensated. Nevertheless, the requirement of  $TVE < 1\%$  is met for all operating points in the ramp, as shown in the bottom plot of Figure 15. The results in actual power system scenarios are presented next.

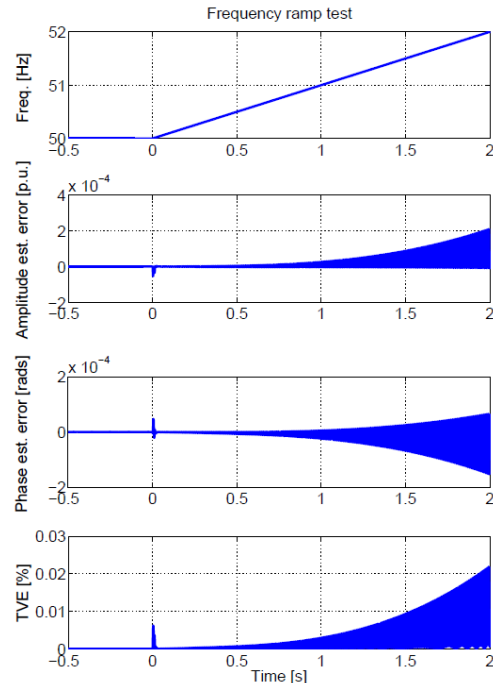


Fig. 15. Frequency ramp, results of the frequency ramp test

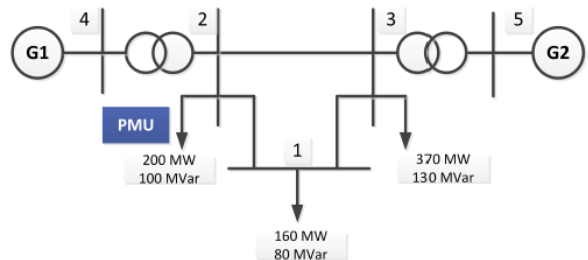


Fig. 16. Case study of generator loss in a five bus network

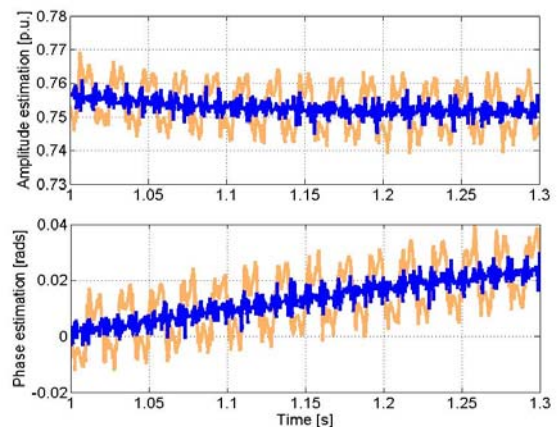


Fig. 17. Amplitude and phase of the voltage phasor at bus 2; the yellow lines represent the estimation of the fundamental only, the blue line includes the second harmonic

The case study consists in the loss of a generator, generator 2 at bus 5, Figure 16 , in a five bus test power network schematically shown in Figure 16 simulated in RTDS.

The voltage phasor measurement at bus 2 is recorded, assuming a voltage sampling rate of 5kHz and SNR = 60dB. Amplitude and phase of the voltage phasor are shown in Figure 17. It can be noticed that the estimation of the second harmonic too (blue line) leads to the best results.

### III. From sensor to sensor system for state estimation

Monitoring the state of the power system in distribution systems the following quantities are of interest:

- Three phase voltage phasor
- Voltage unbalance factor
- Three phase current magnitude

In the state estimation for distribution networks some key decisions must be taken, linked to the peculiarities of these networks, as opposed to the transmission networks, for which state estimation is a well-established practice.

In first place the three-phase state estimator discussed here enables the estimation of the imbalance. This information is relevant especially in those networks with pervasive presence of small, distributed generation, as the case of PV systems in the South of Germany, installed without planning and a priori verifications. The imbalance that appears in this scenario is often detected late, when the conditions for the operation of the protections appear.

In second place, formulate linearized equations of the SE (rectangular coordinates of the state and equivalent current measurements)

Then, various parameters may be subject to optimization in this state estimation, as for example the base power and zero injection accuracy. Many other features of the network operation are still to be investigated in terms of their impact of the location of the instruments. For example one such feature is the inhomogeneous loading, in particular resulting from the presence of the distributed generators.

Finally, because of the size of the problem and of the possible presence of rather variegated local differences, and of the need to reconcile estimations performed e.g. by different companies, a multi area distribution state estimator should be implemented.

For what concerns the three phase state estimation in unbalanced distribution networks, one solution consists in adopting rectangular coordinates of the state and substituting power measurements with equivalent current measurements, as schematically shown in Figure 18.

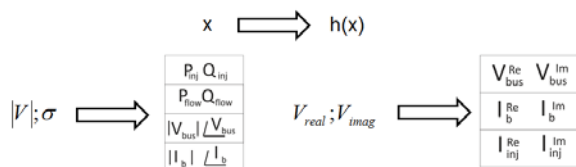


Fig.18. Scheme of the transformation of the state estimation problem

This approach leads to linear state estimation and simpler equations, hence faster solution. Also, this formulation promises to limit the problems of no convergence and to limit ill conditioning issues.

Summarizing the features of the algorithm, we should have:

- Use of three-phase states and three-phase measurements
- Use of three-phase models of the lines

• Use of shunt admittance matrix in the PI model Figure 19

- Use of an optimization process for the choice of
  - Zero injection buses accuracy
  - Base power

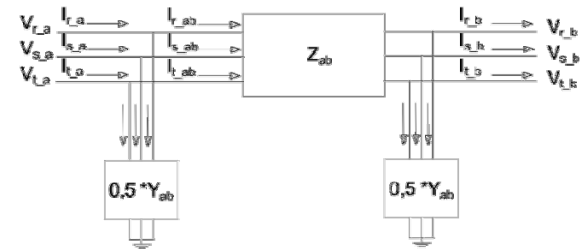


Fig.19. Line model for distribution system

Some more details are provided in the following, with reference to the selection of optimal base power bp and accuracy of the zero power injection error that minimize the state estimation error.

Figure 20 shows the relative error in % of the voltage magnitude versus base power value and power injection accuracy. It can be noticed that, within certain ranges, the relative error decreases significantly.

It is possible to improve the optimization by focusing on the best area, zooming in a smaller area for more refined results, increasing the number of Monte Carlo simulations.

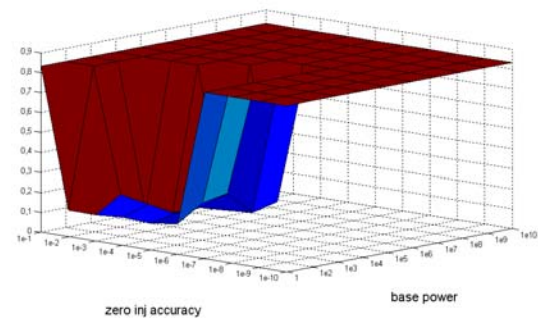


Fig.20. Relative error in % of the voltage magnitude versus base power value and power injection accuracy

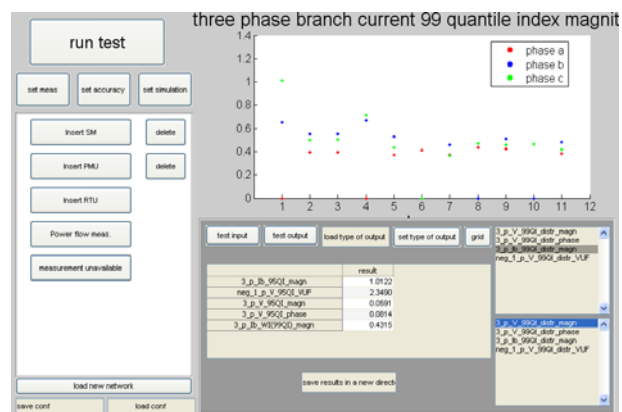


Fig.21. User interface of the tool for instrumentation configuration

The process of assessing the state estimation error that results for a given configuration of instruments, each with given accuracy has been implemented and equipped with a user friendly interface. An example of the appearance of the interface is shown in Figure 21. The interface shows that the user can load a network (e.g. standard or modified IEEE networks), then build the measurement system, by

choosing the position and type of instrument, set the parameters for measurement accuracy and simulation, and eventually calculate and visualize the state estimation error.

As an example, the case of the IEEE 13 bus network is demonstrated here. **Błąd! Nie można odnaleźć źródła odwołania.** shows the network topology and measurement placement, referred to as first scenario.

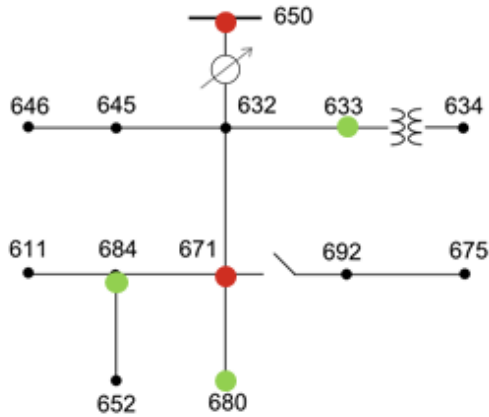


Fig.22. Sample 13 bus network, red dots indicate PMUs, green dots indicate zero power injections

Table 4 shows the values of the parameters used in this example.

Table 4. measurement parameters used in the simulation

PMU	$\epsilon_{magn} = 1\%$ $\epsilon_{ph.angle} = 1\text{crad}$
Pseudo meas.	$\epsilon = 50\%$ ;
Zero injection	$\epsilon = 0,0001\%$ ;
Base power	1 MVA

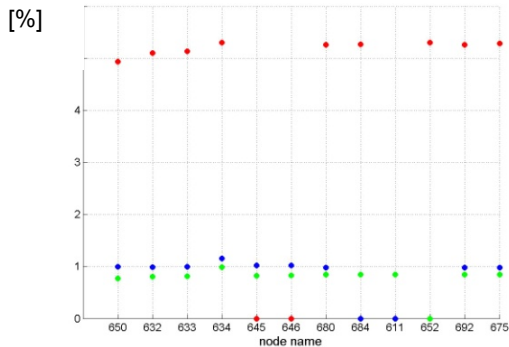


Fig.23. Voltage magnitude error [ % ], bus by bus

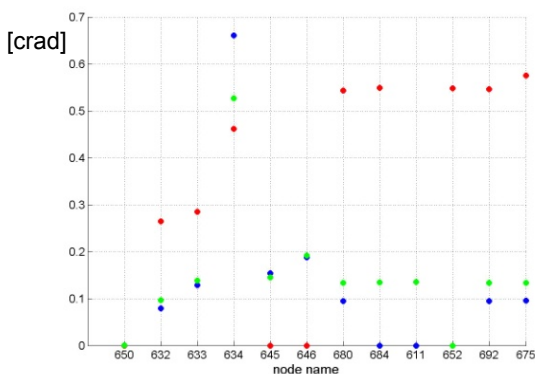


Fig.24. Phase angle absolute error in crad, bus by bus

The results, in terms of voltage magnitude error [%] and phase bus by bus, are shown in Figure 23 and 24. In this case a maximum magnitude error of 1.93% and maximum phase error of 1.75crad were obtained.

Changing the measurement characteristics yields the new scenario, referred to as second scenario, whose parameters are reported in Table 6. The results, in terms of voltage magnitude error [%] and phase bus by bus, are shown in Figure 25 and 26.

A summary of the results is provided in Table 5.

Table 5. : summary of results of SE errors, first scenario, 13 bus network

	Average error in the grid	Maximum error in the grid (99 <sup>th</sup> percentile)
Bus voltage relative magnitude error [%]	2.25	5.33
Bus voltage absolute phase angle error [crad]	0.25	0.69
VUF absolute error [%]	1.44	1.50

Table 6. simulation and measurement parameters of alternative scenario

PMU	$\epsilon_{magn} = 1\%$ $\epsilon_{ph.angle} = 1\text{crad}$
Pseudo meas.	$\epsilon = 50\%$ ;
Zero injection	$\epsilon = 0,01\%$ ;
Base power	1 kVA

A summary of the results for the second scenario is reported in Table 7.

These results provide a quantitative assessment of different measurement characteristics, in term of impact on the accuracy of the state estimation. Tests on the larger 123 bus network, Figure 27, are currently being carried out for the purpose of investigating the impact of the network operating point, the presence of distributed generators, topological changes by opening and closing existing switches for more of less meshed configuration.

Table 7. summary of results of SE errors, second scenario, 13 bus network

	Average error in the grid	Maximum error in the grid (99 <sup>th</sup> percentile)
Bus voltage relative magnitude error [%]	0.64	0.92
Bus voltage absolute phase angle error [crad]	0.15	0.67
VUF absolute error [%]	0.32	0.38

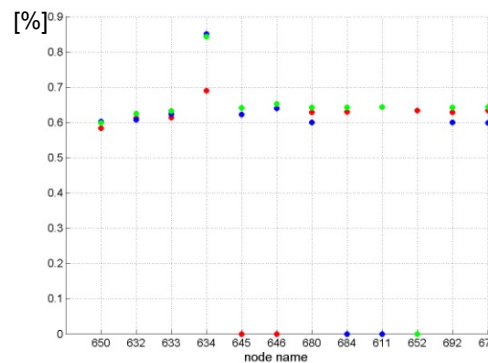


Fig.25. Voltage magnitude error [ % ], bus by bus, for the second scenario

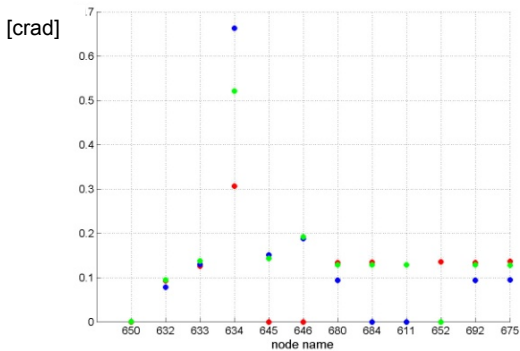


Fig.26. phase angle absolute error in crad, bus by bus, for the second scenario

In the results presented here, focus is on the following quantities:

- Bus voltage magnitude relative error [%]
- Bus voltage phase angle absolute error [crad]
- VUF relative error [%]
- Branch current magnitude relative error [%]

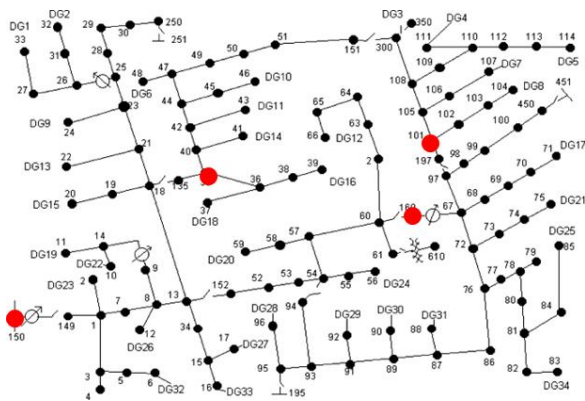


Fig.27. PMU configuration for the 123 node network

The measurement configuration comprises four PMUs (at bus 150, 101, 35, 160), as shown in Figure 27, pseudo measurements, and zero injections with characteristics shown in Table 8.

Table 8. Measurement characteristics for the 123 node network test

Voltage magnitude accuracy	1 %
Voltage phase angle accuracy	1 crad
Pseudo measurement accuracy	50%
Zero injection accuracy	10 <sup>-3</sup> %
Base power	1 MVA

The results obtained with the tool, phase by phase, bus, by bus, are summarized in Table 9. Notice that very large maximum errors, in the order of 100s % have been found in the current estimate of branches that are very lightly loaded (nearly zero actual current).

Table 9. Summary of results for the 123 node network in default conditions

	Average error in the grid	Maximum error in the grid (99 <sup>th</sup> percentile)
Bus voltage relative magnitude error [%]	0.57	1.13
Bus voltage absolute phase angle error [crad]	0.38	0.60
VUF absolute error [%]	0.26	0.40

The unbalance of the distribution network, due for example to the distributed generation, as mentioned before,

can be monitored and tracked before reaching levels that activate the protections.

The same measurement configuration was used to estimate the state of the 123 node network in different scenarios, in particular, in presence of active DGs and in meshed topology, with measurement parameters as in Table 8. For the first case, the results are summarized in Table 10.

Results for the meshed topology are shown in Figure 28, 29, 30. An overall summary of the results is reported in Table 12.

Table 10. Summary of result for 123 node network with DGs

	Average error in the grid	Maximum error in the grid (99 <sup>th</sup> percentile)
Bus voltage relative magnitude error [%]	0.65	1.22
Bus voltage absolute phase angle error [crad]	0.56	1.26
VUF absolute error [%]	0.30	0.42

For the second case, the results are summarized in Table 11.

Table 11. Summary of result for 12 node network in meshed topology

	Average error in the grid	Maximum error in the grid (99 <sup>th</sup> percentile)
Bus voltage relative magnitude error [%]	0.47	0.77
Bus voltage absolute phase angle error [crad]	0.22	0.47
VUF absolute error [%]	0.20	0.25

Table 12. performance of the SE in three scenarios of the 123 node network

123 node network	Maximum voltage magnitude relative error [%]	Maximum voltage phase angle absolute error [crad]	Maximum VUF relative error [%]
default	1,13	0,60	0.40
DGs	1,22	1.26	0,42
meshed	0,77	0,47	0.25

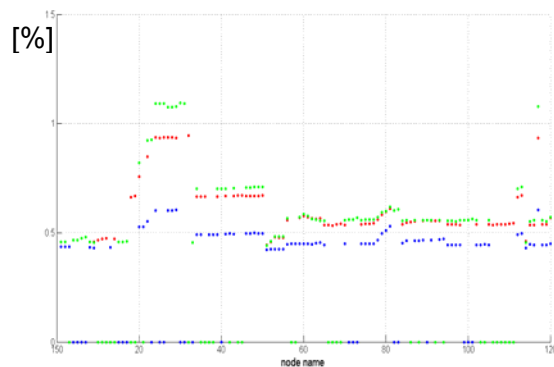


Fig.28. Bus voltage magnitude relative error, bus by bus, for meshed topology

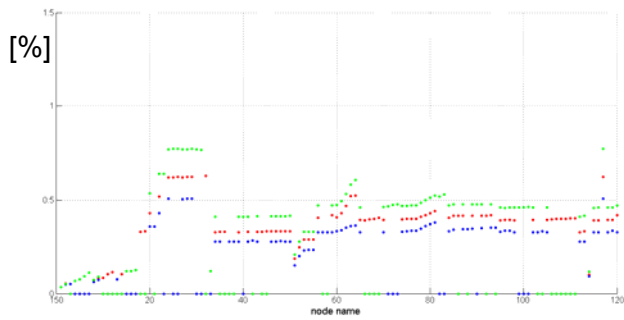


Fig.29. Bus voltage phase angle relative error, bus by bus, for meshed topology

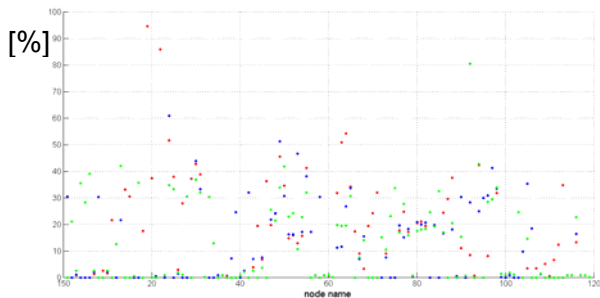


Fig.30. Branch current magnitude relative error, bus by bus, for meshed topology

Finally, the distributed state estimation, and related impact of measurement configuration, has been preliminary analysed.

The multi-area state estimation of distribution networks is of interest particularly in presence of:

- Very large number of buses
- Limitations in hardware computational resources
- Heterogeneous areas in the grid, in terms of topology, ownership
- Tight requirements for maintaining reliability in case of loss of observability

The estimation is performed separately in each area. For the purpose of integrating and aligning the results to a common general reference, one PMU at least is required in each area.

One possible configuration of the multi-area case for the 123 bus network is shown in Figure 31 for sake of example, with no claim that this is the optimized measurement set up.

Preliminary results show that the state estimation is heavily affected by the error of the PMUs in the alignment process. Limited to the accuracy of the estimation, this multi-area state estimator does not produce better results than the centralized estimator for the 123 bus network. However, more extensive analysis is required to account for all other relevant factors.

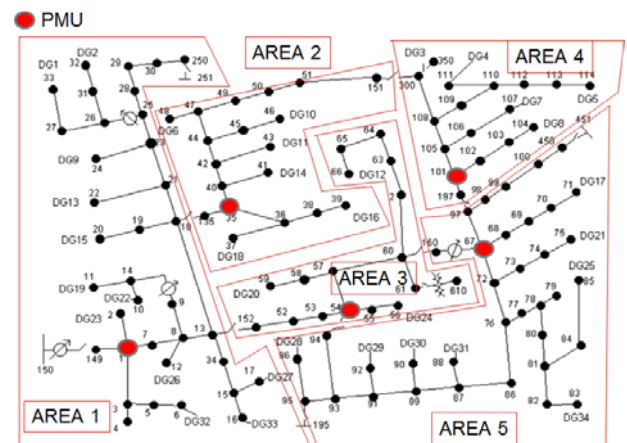


Fig.31. multi-area state estimation in the 123 bus network

The authors want to thank colleagues Prof. Carlo Muscas and Prof. Sara Sulis, University of Cagliari, for the fruitful ongoing collaboration on these research topics.

#### REFERENCES

- [1] J. de la O Serna and J. Rodriguez-Maldonado, "Instantaneous oscillating phasor estimates with Taylor-Kalman filters," *IEEE Transactions on Power Systems*, vol. 26, no. 4, pp. 2336 – 2344
- [2] J. Liu ; F. Ni ; P.A. Pegoraro, F. Ponci, A. Monti, C. Muscas, Fundamental and harmonic synchrophasors estimation using modified Taylor-Kalman filter, *IEEE International Workshop on Applied Measurements for Power Systems (AMPS)*, 2012, Page(s): 1 – 6
- [3] J. Liu ; F. Ni ; J. Tang ; F. Ponci, A. Monti, A modified Taylor-Kalman filter for instantaneous dynamic phasor estimation, *IEEE PES International Conference and Exhibition on Innovative Smart Grid Technologies (ISGT Europe)*, 2012, Page(s): 1 - 7
- [4] *IEEE Standard C37-118-1.2011, C37-119.2-2011*
- [5] A. Angioni, C. Muscas, S. Sulis, F. Ponci, A. Monti, Impact of heterogeneous measurements in the state estimation of unbalanced distribution networks, *IEEE Instrumentation and Measurement Technology Conference (I2MTC) 2013*, Pages: 935-939

**Authors:** Prof. Dr. Antonello Monti, [amonti@eonerc.rwth-aachen.de](mailto:amonti@eonerc.rwth-aachen.de), Prof. Dr. Ferdinanda Ponci, [fponci@eonerc.rwth-aachen.de](mailto:fponci@eonerc.rwth-aachen.de), Junqi Liu, [jliu@eonerc.rwth-aachen.de](mailto:jliu@eonerc.rwth-aachen.de), RWTH Aachen University, Institute for Automation of Complex Power Systems, Mathieustr. 10, 52074 Aachen, Germany  
 Andrea Angioni, [aanqioni@eonerc.rwth-aachen.de](mailto:aanqioni@eonerc.rwth-aachen.de) University of Cagliari, Dipartimento di Ingegneria Elettrica ed Elettronica, Piazza d'Armi, 09123 Cagliari, Italy